Energy of Adhesion of Human T Cells to Adsorption Layers of Monoclonal Antibodies Measured by a Film Trapping Technique

Ivan B. Ivanov,* Asen Hadjiiski,* Nikolai D. Denkov,* Theodor D. Gurkov,* Peter A. Kralchevsky,* and Shigeo Koyasu[#§]

*Laboratory of Thermodynamics and Physico-chemical Hydrodynamics, Faculty of Chemistry, University of Sofia, 1126 Sofia, Bulgaria; [#]Laboratory of Immunobiology, Dana-Farber Cancer Institute and Department of Medicine, Harvard Medical School, Boston, Massachusetts 02115 USA; and [§]Department of Immunology, Keio University School of Medicine, Tokyo 160, Japan

ABSTRACT A novel method for studying the interaction of biological cells with interfaces (e.g., adsorption monolayers of antibodies) is developed. The method is called the film trapping technique because the cell is trapped within an aqueous film of equilibrium thickness smaller than the cell diameter. A liquid film of uneven thickness is formed around the trapped cell. When observed in reflected monochromatic light, this film exhibits an interference pattern of concentric bright and dark fringes. From the radii of the fringes one can restore the shape of interfaces and the cell. Furthermore, one can calculate the adhesive energy between the cell membrane and the aqueous film surface (which is covered by a layer of adsorbed proteins and/or specific ligands), as well as the disjoining pressure, representing the force of interaction per unit area of the latter film. The method is applied to two human T cell lines: Jurkat and its T cell receptor negative (TCR^-) derivative. The interaction of these cells with monolayers of three different monoclonal antibodies adsorbed at a water-air interface is studied. The results show that the adhesive energy is considerable (above 0.5 mJ/m^2) when the adsorption monolayer contains antibodies acting as specific ligands for the receptors expressed on the cell surface. In contrast, the adhesive energy is close to zero in the absence of such a specific ligand-receptor interaction. In principle, the method can be applied to the study of the interaction of a variety of biological cells (B cells, natural killer cells, red blood cells, etc.) with adsorption monolayers of various biologically active molecules. In particular, film trapping provides a tool for the gentle micromanipulation of cells and for monitoring of processes (say the activation of a T lymphocyte) occurring at the single-cell level.

INTRODUCTION

The adhesion of biological cells to other cells, to the extracellular matrix, or to nonliving surfaces is of crucial importance for a variety of biological processes and biomedical applications (Bongrand, 1988; Darnell et al., 1990; Fisher, 1993; Alberts et al., 1994). Typical examples of biological events in which adhesion is of primary importance are cell-cell recognition in organism development, cell migration, immune responses (such as T cell activation or cellular cytotoxic activity of natural killer cells), bacterial invasion of a specific organ, and metastasis of tumor cells.

To analyze the adhesion process of living cells, one should use adequate experimental methods. Several groups of methods are currently used for cell adhesion studies (Bongrand, 1988):

1. Methods based on hydrodynamic flows: flow cytometry, cell detachment from a substrate in a shear flow, etc. In these methods the force that drives the cell attachment/detachment process is created by hydrodynamic fluxes and is usually calculated from the rate of liquid shear and the cell shape (Bongrand et al., 1988; Cozens-Roberts et al., 1990).
2. Micropipette technique, consisting of sucking a portion of the cell membrane into a fine pipette and subsequent micromanipulation. The driving force can be directly measured (after appropriate calibration) if the cell is pushed against a thin flexible platinum fiber, whose deflection is proportional to the applied force. Another possibility is to measure the micropipette suction pressure and to use it to calculate the driving force (Evans, 1988).
3. Electron microscopy and fluorescence methods. The electron microscope provides valuable direct information about the topography of the cell surfaces in the contact zone (Foa et al., 1988). In most cases the cell surface is not smooth, and the presence of numerous microstructures (microvilli) in the zone of intercellular contact can be observed. The electron microscope and the fluorescence methods allow us to investigate the rearrangement of the receptors during the adhesion process. The structural information from these methods complements the results, which are obtained by the other methods.

The results from the experimental studies have led to the conclusion that the cell adhesion is usually governed by two types of interactions: 1) specific receptor-ligand attraction, and 2) nonspecific electrostatic and steric repulsive forces, which are respectively due to the presence of negative charges and hydrophilic polymers (glycocalix) at the cell

Received for publication 21 February 1997 and in final form 13 April 1998.

Address reprint requests to Dr. Peter A. Kralchevsky, Laboratory of Thermodynamics and Physicochemical Hydrodynamics, Faculty of Chemistry, University of Sofia, 1 James Bouchier Ave., 1126 Sofia, Bulgaria. Tel.: 359-2-962-5310; Fax: 359-2-962-5643; E-mail: pk@ltph.bol.bg.

0006-3495/98/07/545/12 $2.00

surfaces. Detailed models of the combined action of these forces were developed by Bell (1978, 1988) (see also Bell et al., 1984; Hammer and Lauffenburger, 1987), and by Evans (1985a,b, 1988). The importance of these interactions (key-lock attraction and nonspecific repulsion) was demonstrated in recent experiments by Leckband et al. (1994), based on precise measurements of the interaction between two lipid bilayers containing streptavidin and biotin (used as a model receptor-ligand pair) performed by means of the surface force apparatus. A notable contribution of the attractive hydrophobic interactions was detected in that study. The much stronger adhesion observed at higher temperatures (above the melting point of the lipid chains) was explained by the enhanced rate of lateral diffusion and molecular rearrangement of the ligands and receptors throughout the lipid membrane (Leckband et al., 1994).

Here we describe another method for investigating the adhesion of living cells to fluid or solid interfaces. We call this method the film trapping technique (FTT) because the cell is trapped within a liquid film of equilibrium thickness smaller than the cell diameter. Thus a Plateau border (a liquid layer of uneven thickness) is formed around each cell (see Fig. 1). By using optical measurements (interferometry in reflected light; Fig. 1 *A*) and the Laplace equation of capillarity, we can resolve the shapes of the air-water and cell-water interfaces. As the cell is pressed between the two film surfaces, it is sharply deformed (Fig. 1 *B*). The contact angle, α, between the air-water and cell-water interfaces is determined. The respective film tension, γ, and the cell membrane tension, σ_C, are two other parameters that are obtained from these measurements. To avoid misunderstandings, let us specify that we will call the air-water-air film in which the cell is captured the "foam film" (Fig. 1 *B*), and we will call the asymmetrical cell-water-air film the "cell-Ab film" (Fig. 1 *C*). From the magnitudes of γ, σ_C, and $\sigma_{W/A}$ (see Fig. 1 *B*) one can calculate the adhesive energy, W, of the cell with the air/water interface covered with an adsorption layer of surface active molecules (e.g., proteins, lipids, glycolipids, etc.) mimicking the surface of another cell (Fig. 1 *C*). In this way the specific ligand-receptor interaction can be studied. In addition, the surface tension of the aqueous solution, $\sigma_{W/A}$, can be independently measured by means of some of the standard methods.

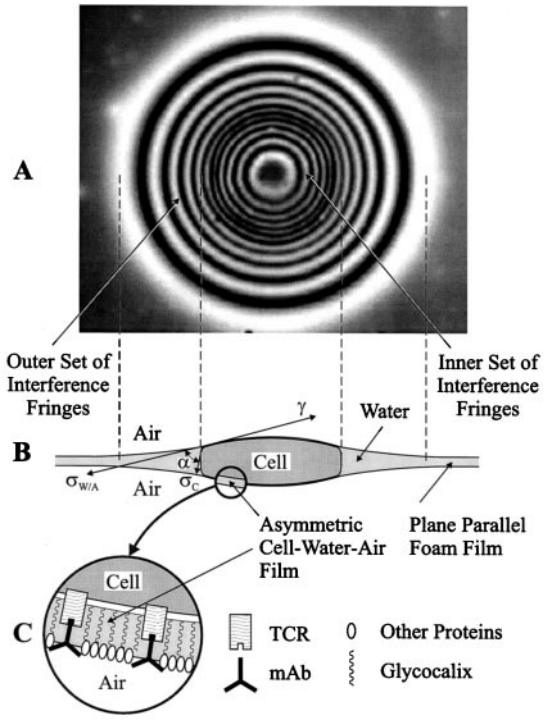

FIGURE 1 Operation principle of the film trapping technique. (*A*) A photograph of a leukemic Jurkat cell trapped in a foam (air-water-air) film containing 10 μg/ml antibody RW28C8 and RPMI 1640 medium. The cell is observed in reflected monochromatic light; a pattern of alternating dark and bright interference fringes appears. (*B*) Sketch of the cell trapped in the film. The fringes are created by the interference of light beams reflected from the two film surfaces (see Fig. 4). The inner set of fringes corresponds to the region of contact of the cell with the protein adsorption layer (*C*). The outer set of fringes is created by the meniscus outside the contact zone. From the radii of the interference fringes one can restore the shapes of the liquid meniscus and of the cell, and calculate the contact angle, α, the cell membrane tension, σ_C, and the tension of the cell-water-air film, γ. From these quantities, the adhesive energy can be calculated.

We apply the FTT to two T cell leukemic lines and investigate their interaction with adsorption layers containing monoclonal antibodies (mAbs). The adhesion of T cells is of particular interest in immunology because 1) the early stage of T cell activation typically requires an adhesion to the antigen presenting cells (APC), and 2) the cytotoxic activity of the natural killer cells is related to their binding to the target cells (Mescher, 1992; Weiss, 1993; Abbas et al., 1994). There are several important properties related to the receptor-ligand interactions and the T cell activation, which could be studied by the FTT, especially when it is combined with fluorescence microscopy (see below). Such are the strengths of the receptor-ligand interaction (energy per one bond); the role of the accessory molecules (CD2, CD4, CD8, etc.) present on the cell surface in the T cell adhesion and activation processes; the relation between kinetics of T cell activation and the cell adhesion, etc. The present study is a first step in that direction, and it is focused mostly on the energy of cell adhesion to the antibody adsorption layers. Some possible developments of the method are briefly discussed at the end of the paper.

In some respects this study is a continuation of our previous work, where the film trapping technique was used for determination of the three-phase contact angle of micrometer-sized solid spheres (latex, silica) of radius between 1 and 10 μm (Hadjiiski et al., 1996). The investigation of deformable particles (such as biological cells) by the FTT requires a much more refined procedure for data analysis, because the shape of the particle is not known in advance and must be determined by calculations based on additional experimental data. From this viewpoint, the generalization of the FTT to living cells is nontrivial, and the analysis is much more complex. Another complication arises from the fact that the biological cells have their own activity, and one

can expect temporal changes in the cell properties, including the energy of adhesion.

The article is organized as follows. The next section describes the experimental procedures and used materials. The third section presents an outline of the procedure for data interpretation. The experimental results are presented and discussed in the fourth section. The derivation of the basic formulas and the numerical algorithm are given as an Appendix.

EXPERIMENTAL

The film trapping technique

The cells are trapped in a horizontal foam film (air-liquid-air) formed in the middle of a biconcave drop of cell suspension, which is placed in a vertical cylindrical glass capillary (Fig. 2). The film is created by sucking out the liquid through an orifice in the capillary wall (Scheludko and Exerowa, 1959). The amount of liquid in the capillary and the capillary pressure of the Plateau border (biconcave drop) encircling the film can be varied by a pressure control system. The latter consists of a syringe, connected to a micrometric screw, which allows precise ejection or injection of liquid into the capillary. P_A, P_W, and P_C denote the pressure inside the air, water, and cell, respectively. During the experiment we control the pressure drop across the water-air interface, $\Delta P_{W/A} = (P_A - P_W)$ (Fig. 3), by sucking out small amounts of water from the plateau border surrounding the foam film (which leads to an increase in $\Delta P_{W/A}$) or by injection of water back into the Plateau border (decreasing $\Delta P_{W/A}$). The liquid (air-water-air) films were rather stable, because of the presence of adsorbed protein layers at the film surfaces. Several cycles of consecutive increasing and decreasing of capillary pressure were possible before rupturing of the liquid film. The duration of such a cycle was typically around a couple of minutes.

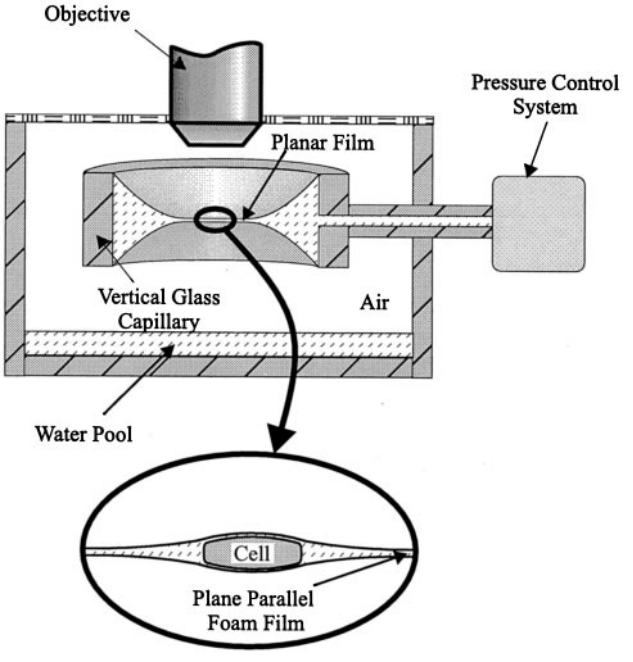

FIGURE 2 Scheme of the experimental set-up. A planar foam film is formed in a vertical glass capillary by sucking out liquid through an orifice in the capillary wall. By changing the amount of liquid in the capillary one controls the film radius, the shape of the meniscus surrounding the film, and the capillary pressure, $\Delta P_{W/A}$. The trapped cells are observed with a microscope in reflected light. The capillary is enclosed in a glass container to prevent water evaporation from the film; a water pool ensuring saturation of the vapor covers the bottom of the container.

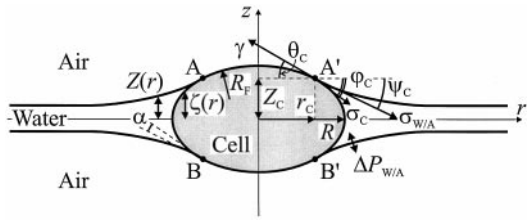

FIGURE 3 Schematic cross section of a cell trapped in a foam film. R denotes the equatorial radius of the deformed drop, r_C is the radius of the contact line, R_F is the radius of curvature of the film, formed between the cell membrane and the protein adsorption layer. $Z(r)$ and $\zeta(r)$ are the generatrices of the air-water and cell-water interfaces. $\Delta P_{W/A} = (P_A - P_W)$ is the capillary pressure across the water meniscus.

The cells trapped in a liquid film are observed from above (Axioplan Zeiss microscope, 50× LD Epiplan objective) in reflected monochromatic light of wavelength $\lambda_0 = 546$ nm. Under these conditions the image of the cell and the surrounding Plateau border contain a number of concentric consecutive bright and dark fringes (see Fig. 1 *A*). Each dark (bright) fringe is due to destructive (constructive) interference of the light beams reflected from the upper and lower film surfaces (Born and Wolf, 1993). The transition from one dark to the closest bright fringe (or vice versa) corresponds to a variation in the water layer thickness equal to $\lambda_0/4n_W = 102$ nm (n_W is the refractive index of the water solution). One can distinguish two different sets of interference fringes: 1) an inner set, which is due to the light reflected from the lower and upper spherical films that cover the cell (contact zone); 2) an outer set, which is due to the interference of light reflected from the upper and lower water-air interfaces around the cell (outside the contact zone). The interference pattern is observed and recorded by CCD camera (Panasonic WV BP500) and video recorder. The video records are later processed to restore the shapes of the film surfaces and of the cell. The theoretical interpretation of the recorded interference pattern is described in the next section.

Before the experiments are performed, the cells suspended in RPMI 1640 (also containing 10% fetal calf serum) are stained with 10 μg/ml monoclonal antibody on ice for 30 min. The cooled suspension is loaded into the experimental cell (Fig. 2), and the experiment (the formation of film by ejection of solution) starts 10–20 min after that moment. During this period the suspension warms up to room temperature, and adsorption of surface-active molecules (such as serum proteins, mAbs, etc.) at the air-water interface takes place.

The surface tension, $\sigma_{W/A}$, of the protein solutions (needed for the calculations) was measured by the Wilhelmi plate method (see, e.g., Adamson, 1976) on a digital tensiometer K10T (Krüss, Germany). For our system we measured $\sigma_{W/A} = 56$ mN/m. All experiments were performed at room temperature, 24° ± 1°C.

Materials

Two T cell lines were used: 1) human T cell leukemic line Jurkat, and 2) T cell receptor negative (TCR^-) variant of Jurkat named 31.13 (Alcover et al., 1988). The cell lines were grown in RPMI 1640 medium, supplemented with 10% fetal calf serum, 4 mM L-glutamine, 50 units/ml penicillin G, 50 μg/ml streptomycin, and 10 mM HEPES buffer. The cells were cultured at 37°C in humidified atmosphere containing 5% CO_2 and 95% air. Typically, the suspensions reach a confluent stage (10^6 cells/ml) in 3 days, and afterward the cells should be diluted into a new medium. We studied the interaction of these cells with adsorption layers containing three different mAbs: 5Rex9H5, which is a specific mAb against the Jurkat TCRβ (Acuto et al., 1983); RW28C8, specific for the CD3ε subunit and thus also binding to TCR (Meuer et al., 1983); and 1η4F2, a negative control (Hussey et al., 1993).

THEORETICAL INTERPRETATION OF THE INTERFERENCE PATTERN

In this section we briefly describe the procedure for data interpretation. Only the main steps of the procedure are outlined here; the complete theoretical analysis of the interference pattern is presented in the Appendix.

As mentioned above, the fringes (Fig. 1 *A*) are due to the interference of the light beams reflected from the two film surfaces (Fig. 4). The condition for destructive or constructive interference of these two beams is related to the difference in their optical paths, i.e. to the local film thickness (see the Appendix for details). From the recorded image one can determine the radial coordinate, r_k, of each fringe of order k, which corresponds to a given local film thickness, Z_k (Fig. 5).

To find the shape of the air-water interface, we have to interpolate these points by the respective theoretical function. In our case this theoretical function has to be a solution of the Laplace equation of capillarity:

$$\frac{1}{R_1} + \frac{1}{R_2} = \frac{\Delta P_{W/A}}{\sigma_{W/A}} \tag{1}$$

(along with the respective boundary conditions). Here $\Delta P_{W/A} = (P_A - P_W)$ is the capillary pressure drop between the aqueous and the gaseous phases, $\sigma_{W/A}$ is the surface tension of the aqueous solution, and R_1 and R_2 are the two principal radii of curvature of the interface (Princen, 1969; Kralchevsky et al., 1997). In general, R_1 and R_2 are different ($R_1 = R_2$ for spherical surface only) and may vary throughout the interface.

The inner and outer sets of fringes, distinguishable in Fig. 1 *A*, correspond to two different solutions of the Laplace equation of capillarity—the inner set corresponds to the region of contact of the cell with the foam film surface, whereas the outer set corresponds to the air-water interface, which is outside the contact zone.

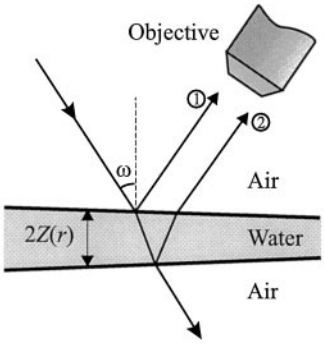

FIGURE 4 Light beams reflected from the upper and lower surfaces of a thin water layer interfere to create the pattern in Fig. 1 *A*. Constructive or destructive interference is observed, depending on the difference in the optical paths of the two beams, i.e., on the film thickness, $2Z(r)$. In our case the angle of incidence of the illuminating beam is $\omega = 0$, and the positions of the fringes are determined by Eq. A.1 (see, e.g., Born and Wolf, 1993).

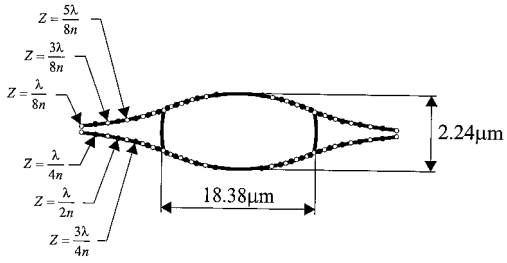

FIGURE 5 Reconstructed profile of the interfaces from the image shown in Fig. 1 *A*. The experimental points correspond to the positions of the maxima (*empty circles*) and minima (*black dots*) in the intensity of the reflected light, as measured from the digitized image (cf. Eq. A.1).

Shape of the meniscus around the cell (outer set of fringes)

Details of the numerical procedure used to restore the meniscus profile are described in the Appendix. As a final output of this procedure, we obtain the value of the capillary pressure, $\Delta P_{W/A}$, and a theoretical function that interpolates the coordinates of the outer set of fringes $Z_k(r_k)$, as determined from the digitized images (see Fig. 1 *A*). The experimental data and the best fit for one of the cells are presented in Fig. 5.

The three-phase contact line (of diameter $2r_C = 18.38$ μm in Fig. 5) represents the line of intersection of the outer meniscus with the cell membrane.

Shape of the cell-Ab film (inner set of fringes)

The real thickness of the cell-Ab films (the arcs AA' and BB' in Fig. 3; see also Fig. 1 *C*) is expected to be ~20–50 nm, because these films are stabilized by the protein adsorption layer at the air-water interface and by the glycocalix covering the cell membrane. To describe these films we use the so-called membrane approach to the thermodynamics of thin liquid films (see, e.g., Ivanov and Kralchevsky, 1988). The membrane approach formally treats the liquid film as a mathematical surface of zero thickness. At the contact line, $r = r_C$, this surface (AA' or BB') meets the cell-water surface, $\zeta(r)$, and the outer water-air meniscus, $Z(r)$ (Fig. 3). The solution of the Laplace equation of capillarity for each of the two caps (AA' or BB' in Fig. 3), at negligible gravity, represents a portion of a sphere (Princen, 1969). Its radius of curvature, R_F, and the position of its geometrical center can be determined from the inner set of interference fringes in Fig. 1 *A* (see the Appendix for details).

Having found the value of R_F and the shape of the outer meniscus (previous subsection), we can calculate the coordinates, r_C and Z_C, of the point of intersection of these two surfaces, as well as the slope angles at the contact line, ψ_C and θ_C (Fig. 3).

Shape of the cell membrane outside the contact zone

Because of the axial symmetry of the system, the shape of the cell-water interface is described by the generatrix $\zeta(r)$ (Fig. 3). The function $\zeta(r)$ is also a solution to the Laplace equation of capillarity. As shown in the Appendix, from the available experimental data, one can determine $\zeta(r)$, the pressure difference across the cell membrane, $\Delta P_{C/W} = (P_C - P_W)$, and the membrane tension, σ_C. The final result for $\zeta(r)$ reads

$$\zeta(r) = R\int_0^{\Phi} \frac{1 - bm\sin\Phi}{b\sqrt{1 - m\sin^2\Phi}}\,d\Phi = R[E(\Phi, m) - \sqrt{1-m}F(\Phi, m)] \tag{2}$$

where R is the equatorial radius of the deformed cell (Fig. 3), whereas $F(\Phi, m)$ and $E(\Phi, m)$ are elliptic integrals of the first and second kind, respectively, defined as follows (Abramowitz and Stegun, 1964):

$$F(\Phi, m) \equiv \int_0^{\Phi} \frac{dx}{\sqrt{1 - m\sin^2 x}} \qquad 0 < m < 1 \tag{3}$$

$$E(\Phi, m) \equiv \int_0^{\Phi} \sqrt{1 - m\sin^2 x}\,dx$$

The constants b and m and the variable Φ are defined by the expressions

$$b \equiv \frac{\Delta P_{C/W} R}{2\sigma_C} \tag{4}$$

$$m\sin^2\Phi \equiv 1 - \frac{r^2}{R^2} \tag{5}$$

$$m \equiv \frac{2b - 1}{b^2} \tag{6}$$

The volume of the cell can be found by integration of the profile, $\zeta(r)$:

$$V = 2\pi\int_R^{r_C} r^2 \frac{d\zeta}{dr}\,dr + 2V_{SC}, \tag{7}$$

where V_{SC} is the volume of one of the spherical caps of the cell (above and below the planes AA' and BB' in Fig. 3). Using Eq. 2, one obtains

$$V = \frac{2\pi R^3}{3}[(4 - 2m - 3\sqrt{1-m})E(\Phi_C, m) - (1-m)F(\Phi_C, m) + (m/2)\sin(2\Phi_C)\sqrt{1 - m\sin^2\Phi_C}] + \frac{2\pi}{3}[2R_F^2(R_F - \sqrt{R_F^2 - r_C^2}) - r_C^2\sqrt{R_F^2 - r_C^2}] \tag{8}$$

where $\Phi_C = \Phi(r_C)$ (Eq. 5).

The expressions, describing the shape of the cell membrane, contain three unknown parameters: the equatorial radius of the deformed cell, R; the membrane tension, σ_C; and the capillary pressure drop across the cell membrane, $\Delta P_{C/W}$. In principle, one can measure directly the equatorial radius, R, by microscope, and use it as an input parameter for determination of the membrane shape and of the values of the other quantities. However, our numerical calculations showed that the accuracy of the optical measurement of R is insufficient for that purpose. A very small variation in the value of R (within ± 100 nm, which is below the resolution of the optical microscope) leads to a large variation in the calculated values of all other parameters, or even to the absence of a solution of the Laplace equation that satisfies the requirement for intersection of the water-air interface with the cell surface at the contact line (see Eq. A.11 in the Appendix).

To overcome this problem, we used a more complex (but more accurate) procedure. We formulated a set of several equations that must be solved numerically to calculate R and to describe completely the geometry of the system (see the Appendix). As a final output of the numerical procedure, we determine the values of the membrane tension σ_C, the tension of the spherical caps, γ, the capillary pressure, $\Delta P_{C/W}$, the equatorial radius, R, and the membrane slope angle at the contact line, φ_C (Fig. 3). It always turns out that the calculated values of R agree very well with the experimentally measured ones. The contact angle, α, formed at the contact line is equal to

$$\alpha = \varphi_C - \psi_C \tag{9}$$

Thus the geometrical configuration of the system is completely resolved, and the membrane tensions σ_C and γ are determined.

ADHESION ENERGY: RESULTS AND DISCUSSION

Determination of the adhesion energy and the disjoining pressure

The interaction of the cell with the protein adsorption layer can be characterized by two thermodynamic quantities: the adhesion energy per unit area of the cell-Ab film, W (see Fig. 1 *C*), and the force per unit area of this film, Π. The latter is usually called "disjoining pressure" (Derjaguin, 1989; de Feijter, 1988).

By definition, the energy (work) of adhesion is (Adamson, 1976; Israelachvili, 1992)

$$W = \sigma_{W/A} + \sigma_C - \gamma \tag{10}$$

Note that W does not coincide with the interaction free energy of the film, Δf, which is another quantity used in the thermodynamics of thin liquid films (Ivanov and Toshev, 1975; de Feijter, 1988; Kralchevsky et al., 1995). The

relationship between W and Δf is given by the expression

$$W \equiv -(\Delta f + \Pi h); \qquad \Delta f \equiv \int_h^\infty \Pi(h)\mathrm{d}h \qquad (11)$$

where h is the thermodynamic thickness of the film. The term Πh on the right side of Eq. 11 is usually negligible compared to Δf, and hence $W \approx -\Delta f$.

On the other hand, the disjoining pressure (surface force per unit area) that stabilizes the cell-Ab films at the caps of the cell (Fig. 1 *C*) can be found from the pressure balance at the upper film surface:

$$\Pi \equiv \frac{2\sigma_{W/A}}{R_F} + \Delta P_{W/A} = \frac{2\sigma_{W/A}}{r_C}\sin\theta_C + \Delta P_{W/A} \qquad (12)$$

Equation 12 results from the definition of Π as the excess pressure in the cell-Ab film, with respect to the pressure in the Plateau border around the cell (Derjaguin, 1989; Ivanov and Kralchevsky, 1988). All parameters appearing in Eq. 12 are determined by means of the numerical procedure described in the Appendix. Note that in our systems the disjoining pressure, Π, is positive (i.e., it corresponds to repulsion between the two film surfaces), and consequently, it stabilizes the cell-Ab film in Fig. 1 *C*. Thus we calculate the basic parameters, W and Π, characterizing the adhesion of the T cell to the antibody adsorption layer.

Numerical results

As explained in the second section, we could perform several consecutive cycles of increasing and decreasing the capillary pressure, $\Delta P_{W/A}$, with a given film before its rupture. Higher values of the capillary pressure mean that the captured cell is pressed harder between the film surfaces. In Fig. 6, *A* and *B*, we plot the resolved shape of a Jurkat cell (this is the same cell, which is shown in Fig. 1 *A*), trapped in a liquid film containing 10 μg/ml RW28C8, at two different capillary pressures, $\Delta P_{W/A} = 25$ and 110 Pa. One sees in Fig. 6 that the cell is flattened to a greater extent at the higher capillary pressure, $\Delta P_{W/A}$. The radius of the contact region also increases.

In Fig. 6, *C* and *D*, we compare the shapes of two different cells in the presence and in the absence of a binding antibody at the same capillary pressure, $\Delta P_{W/A} \approx$ 175 Pa. There is a pronounced difference in the region of the contact line: the contact angle, α, is much larger in the presence of a binding antibody. Moreover, the cell deformation is larger (the cell is more flattened) in the latter case.

In Table 1 we show a more complete set of results for the cell shown in Fig. 1 *A*. These results are obtained from the analysis of 11 images taken at different moments within one cycle of the pressure change. The results are shown in chronological order. One sees in the first column of Table 1 that the capillary pressure, $\Delta P_{W/A}$, initially increases and then decreases. As seen from the table, the geometrical area of the cell increases with the compressing pressure, $\Delta P_{W/A}$,

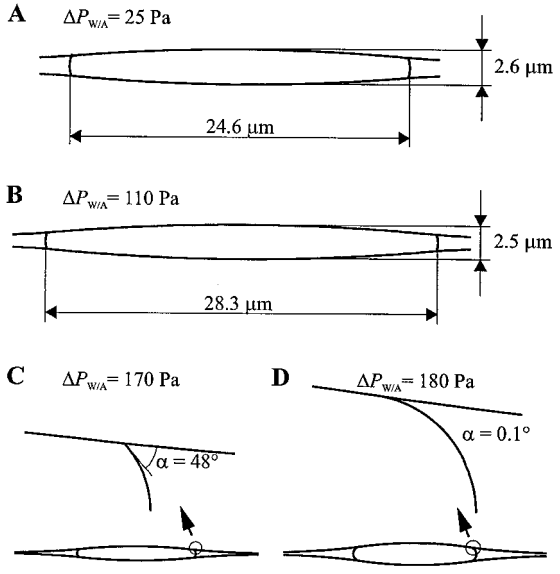

FIGURE 6 Reconstructed geometry of leukocytes trapped in liquid films. Cross section of a cell (the one shown in Fig. 1 *A*) at two different values of the capillary pressure. (*A*) $\Delta P_{W/A} = 25$ Pa; (*B*) $\Delta P_{W/A} = 110$ Pa. The shapes of two different cells at the same capillary pressure, $\Delta P_{W/A} \approx$ 175 Pa, in the presence of a binding antibody RW28C8 (*C*) and in the presence of a nonbinding antibody 1η4F2, which is a negative control (*D*), are also shown.

which is probably due to an additional unruffling of the cell membrane. This trend is illustrated in Fig. 7, where the area of the cell is plotted as a function of the capillary pressure. The circles are experimental data, and the straight line is plotted by the least-squares method. Note that ~90% of the cell membrane is in contact with the adsorption monolayer at the air-water interface (cf. the third and fourth columns in Table 1). Furthermore, the area of the deformed cell is about two times larger than the apparent surface area of a sphere of the same volume. A similar result (about a twofold increase in the apparent membrane area) was obtained previously with neutrophils and other leukocytes, by using rapid osmotic swelling and the micropipette technique (Chien et al., 1987).

At first glance, it can be surprising that the calculated volume of the cell also increases slightly with the capillary pressure (Table 1). One could expect that the stronger pressing of the cell between the surfaces of the liquid film would act to squeeze out some amount of water from the cell cytoplasm into the surrounding aqueous solution. The cell is probably able to actively control the transport of liquid through the cytoplasmic membrane to resist the increased pressure.

The radius of the contact line, r_C, and the equatorial radius of the cell, R, increase (although slightly) with the increase in the capillary pressure, $\Delta P_{W/A}$, as expected (see Table 1). On the other hand, there is no detectable systematic variation in the radius of the spherical caps, R_F, of the contact angle, α, of the cell membrane tension, σ_C, or of the adhesive energy, W, with $\Delta P_{W/A}$ in the framework of experimental accuracy (Table 1). The dependence of the cap-

TABLE 1 Parameters characterizing a trapped Jurkat cell at different values of the compressing capillary pressure, $\Delta P_{W/A}$, in a film from RPMI 1640 medium, containing 10 μg/ml antibody RW28C8

$\Delta P_{W/A}$ (Pa)	Volume (μm^3)	Area (μm^2)	Caps area (μm^2)	r_C (μm)	R (μm)	R_F (μm)	$\Delta P_{C/W}$ (Pa)	Π (Pa)	σ_C (mN/m)	α (deg)	W (mJ/m^2)
61.5	981	1082	968	12.40	12.52	131	924	914	1.68	68.1	1.03
110.4	1165	1353	1243	14.05	14.14	152	853	847	1.57	72.2	1.07
110.1	1177	1376	1267	14.19	14.27	154	842	836	1.54	72.3	1.05
91.4	1137	1243	1130	13.39	13.49	131	954	945	1.87	71.1	1.24
69.5	1042	1126	1009	12.66	12.78	129	948	938	1.69	67.6	1.03
67.6	1071	1178	1061	12.98	13.09	140	876	868	1.71	70.2	1.11
33.6	1018	1109	990	12.54	12.66	141	836	827	1.69	69.4	1.07
33.5	984	1075	955	12.32	12.45	143	828	819	1.62	68.4	1.00
33.0	954	1042	921	12.10	12.24	143	825	816	1.54	67.0	0.92
24.7	953	1052	934	12.18	12.30	142	820	811	1.75	70.4	1.14
29.5	947	1044	926	12.13	12.25	142	825	816	1.67	69.4	1.06

The surface tension of the aqueous solution is $\sigma_{W/A} = 56$ mN/m. The data are presented in chronological order.

illary and disjoining pressures, $\Delta P_{C/W}$ and Π, on $\Delta P_{W/A}$ is also complicated (see Table 1), which might be related to the biological activity of the cell. We have not noticed an appreciable tendency such as hysteresis in the variation of the calculated parameters in the consecutive cycles and with the direction of the capillary pressure variation (increase or decrease in $\Delta P_{W/A}$).

In Fig. 8 the adhesive energy, W (calculated from Eq. 10), is shown as a function of the capillary pressure, $\Delta P_{W/A}$. The solid line is plotted according to the least-squares method. As seen from the figure, there is a very slight trend toward an increase in W with the capillary pressure, but this effect is practically in the limits of experimental accuracy. The adhesive energy is relatively high ($W = 1.07 \pm 0.08$ mJ/m^2), which is most probably due to the high affinity of the T cell receptors (TCR) for the RW28C8 mAbs adsorbed at the air-water interface. As known, RW28C8 is a specific ligand for Jurkat TCR, because it binds to CD3ε. The energy per one ligand-receptor bond, E_B, can be roughly estimated if one divides W by the surface density of TCR ($\approx 5 \times 10^{15}$ m^{-2}). The result of this estimate is $E_B \approx 2 \times 10^{-19}$ J (30 kcal/mol or 50 k_BT, where k_BT is the thermal energy, and k_B is the Boltzmann constant). The reproducibility of the mean values of W from measurements with different cells of the same line is typically within $\pm 30\%$.

The calculated tension of the cell membrane is $\sigma_C = 1.67 \pm 0.10$ mN/m. This relatively high value could be explained by the substantial deformation of a cell trapped in the film. The flattening of the cell leads to unruffling and stretching of the cell surface and to a corresponding increase in the membrane tension. At the highest values of the capillary pressure, $\Delta P_{W/A}$, we sometimes observed disruption of the cytoplasmic membrane and lysis of the cells.

One should note that the variation in the capillary pressure, $\Delta P_{W/A}$, is in a relatively wide range, typically between 20 and 150 Pa. However, the disjoining pressure, Π, which stabilizes the cell-Ab film, varies in a relatively narrow range for a given cell (see Table 1). Indeed, the disjoining pressure depends mainly on the curvature of the cell-Ab film (see Eq. 12, where the term $\Delta P_{W/A}$ turns out to be an order of magnitude smaller than the other term); consequently,

$$\Pi \propto \frac{1}{R_F}$$

The calculations show that in our experiments, R_F varies in a relatively narrow range for a given cell, and hence Π changes slightly. The same is true for the capillary pressure $\Delta P_{C/W}$ (note that $\Pi \approx \Delta P_{C/W}$; Table 1). On the other hand,

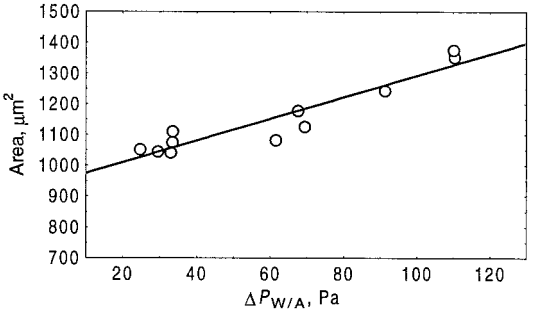

FIGURE 7 Area of the surface of a Jurkat cell as a function of the applied capillary pressure, $\Delta P_{W/A}$ (the data are for the cell shown in Fig. 1 *A*). The circles are obtained from the analysis of recorded images, and the straight line is plotted by the least-squares method.

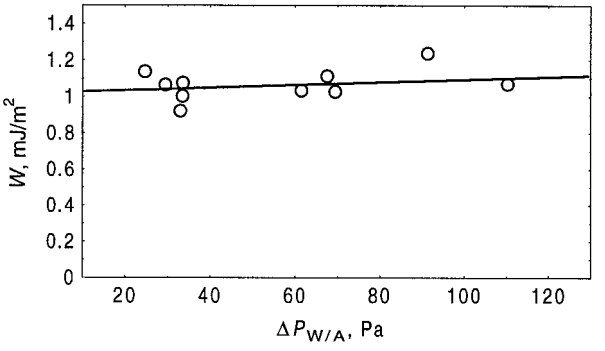

FIGURE 8 Energy of adhesion, W, as a function of the capillary pressure, $\Delta P_{W/A}$, for the cell shown in Fig. 1 *A*. The circles are obtained from image analysis, and the straight line is plotted by the least-squares method.

the disjoining pressure is substantially different for cells of different size—the larger the cells, the lower the disjoining pressure. For instance, in an experiment with a larger Jurkat cell (compared to that discussed above) at similar compressing pressure, $\Delta P_{W/A} \approx 60$ Pa, we determined $R \approx 17$ μm, $\Pi \approx \Delta P_{C/W} \approx 600$ Pa.

The arithmetic mean values (averaging over various studied cells) of the adhesive energy, W, for each of the two cell lines and for adsorption layers containing various mAbs are listed in Table 2. As seen, measurable interaction energy is observed only when Jurkat cells are in contact with adsorption layers of 5Rex9H5 and RW28C8 Abs. The cells from the TCR deprived line (31.13) do not interact specifically with any of the Abs (the last column of Table 2). Similarly, the 1η4F2 Ab, which is a negative control, does not show measurable adhesion energy with any of the cell lines (see the last row in Table 2).

The fact that the adhesion energy depends so strongly on the type of Ab used demonstrates that a sufficiently large portion of the Ab molecules do not loose their binding activity upon adsorption at the water-air interface (see Fig. 1 *C*). In fact, the detailed structure of the adsorption layer (containing serum proteins and Ab molecules) is not clear at present. The structure shown in Fig. 1 *C* implies that the serum proteins and the Ab molecules are both in contact with the air phase. It is possible that the serum molecules adsorb first at the air-water interface (because of their higher concentration and faster diffusion), thus forming a relatively dense adsorption layer, whereas the Ab molecules form a second adsorption layer beneath that of the serum proteins. Further studies by other methods (e.g., ellipsometry or specular reflectivity of neutrons) could be of substantial help in clarifying the real structure of the adsorption layer.

We should note that the reproducibility of the determined adhesive energy from the experiment with a given cell was typically between ± 0.1 and ± 0.4 mJ/m^2 (see Tables 1 and 2). The reproducibility of the mean value from measurements with different cells interacting with a monolayer of a given Ab was approximately the same. Furthermore, in the cases in which the adhesive energy was relatively small (below ~ 0.2 mJ/m^2), the calculated mean value was within the limits of the experimental error. The latter cases are indicated in Table 2 as $W \approx 0$. We are currently elaborating the procedure of data interpretation to further improve (if possible) the accuracy of the determined adhesive energy (see also Accuracy of the Numerical Procedure Used for Data Interpretation, below).

TABLE 2 Energy of adhesion, *W*, of the cells from two cell lines to adsorption layers containing different mAbs

	Average adhesive energy, W (mJ/m^2)	
Abs	Jurkat	31.13
RW28C8	0.85 ± 0.25 (2/32)	≈ 0 (2/20)
5Rex9H5	0.77 ± 0.40 (2/46)	≈ 0 (3/30)
1η4F2	≈ 0 (1/16)	≈ 0 (2/20)

The figures in parentheses show the number of cells studied and the number of analyzed images, respectively. With $W \approx 0$, we indicate the cases in which the interaction energy was below ~ 0.2 mJ/m^2, and the calculated average value was within the limits of the experimental error.

CONCLUSIONS AND PROSPECTS FOR FUTURE WORK

The main conclusions from the present study can be summarized as follows:

A novel method for investigation of the adhesion of biological cells to protein monolayers, adsorbed at an air-water interface, is proposed (Figs. 1 and 2). The method is called the film trapping technique, because the cells are trapped in a liquid film of equilibrium thickness smaller than the cell diameter. The shape of the cell and the adhesive energy are determined from analysis of the interference pattern, which appears when a captured cell is observed in reflected monochromatic light (Figs. 4 and 5). The basic formulas describing the system are derived; numerical algorithms and computer programs for analysis of the interference pattern are developed (see the Appendix).

The method allows us to determine the thermodynamic quantities characterizing the microscopic film, which appears at the contact of the cell with the Ab-monolayer adsorbed at the water surface (Fig. 1 *C*); these are the adhesive energy, disjoining pressure, film tension, contact angle cell-meniscus, etc. An important feature of our method is the ability to manipulate the captured cell by controlling the force that presses the cell against the Ab adsorption monolayer (the capillary pressure, $\Delta P_{W/A}$). Thus changes in the cell volume, area, and membrane tension can be determined as functions of the applied capillary pressure (Table 1 and Fig. 9).

A comparative study of the interaction of two cell lines with three types of adsorption monolayers of monoclonal antibodies is performed (Table 2). The results show that appreciable adhesive energy is obtained when the cells interact with the adsorption monolayers containing antibodies specific for the cell receptors. Otherwise, the interaction energy is zero in the framework of experimental accuracy.

The method can be further developed to perform observations of biological cells in fluorescent light. For example, this would allow us to investigate the early events of T cell activation by recording the Ca^{2+} mobilization in real time at the single-cell level. Another possibility is to examine whether and how reorganization of the receptors takes place in the region of contact during the cell activation (for this purpose fluorescinated mAbs should be used). Alternatively, the receptor distribution along the cell surface can be studied by combining the FTT with the method of cryoelectron microscopy. As recently shown (Denkov et al., 1996), macroscopic foam films, like those used in the FTT, can be vitrified by ultrarapid freezing and then investigated by cryoelectron microscopy.

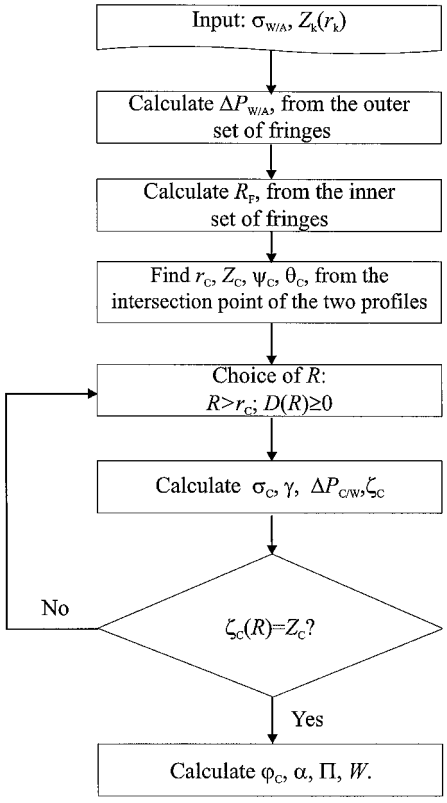

FIGURE 9 Block scheme of the numerical procedure for data interpretation.

APPENDIX: INTERPRETATION OF THE INTERFERENCE PATTERN

The bright and dark fringes seen in Fig. 1 *A* are created by the interference of the light beams reflected from the two foam film surfaces (Fig. 4). The extrema in the intensity of the reflected light correspond to the condition (Born and Wolf, 1993)

$$Z_k = k\frac{\lambda_0}{8n_W}, \qquad k = 0, 1, 2, \ldots \tag{A.1}$$

where Z_k is half of the local thickness of the water film. Here k is the order of interference (k is odd for the bright fringes and even for the dark fringes); n_W denotes the refractive index of the aqueous phase. From the recorded images one can determine the radial coordinate, r_k, corresponding to each fringe of order k. We developed an image analysis computer program, which calculated the intensity of the reflected light averaged over a circumference, centered at the axis of symmetry of the interference pattern. In this way a precise determination of the radii of the interference minima and maxima is accomplished, i.e. the coordinates, Z_k and r_k, of a number of points from the meniscus surface are found.

Shape of the meniscus around the cell (outer set of fringes)

The numerical calculations (see Table 1) showed that in our experiments, the capillary pressure, $\Delta P_{W/A}$, is typically on the order of 100 Pa. On the other hand, the pressure difference across the air-water interface, created by gravity, is on the order of $\Delta\rho_{W/A}gZ_C \approx 10^{-2}$ Pa, i.e., four orders of magnitude lower (Z_C is the height of the contact line with respect to the midplane of the foam film; Fig. 3). Therefore, we can neglect the effect of gravity in the calculations without any loss of accuracy. Moreover, we can consider the system as being symmetrical with respect to the horizontal midplane of the large foam film in which the cell is trapped. The Laplace equation of capillarity, which describes the shape of the water-air outside the contact zone interface (at negligible gravity), can be written in the form (see, e.g., Princen, 1969; Kralchevsky et al., 1997)

$$\frac{d\sin\psi}{dr} + \frac{\sin\psi}{r} = \frac{\Delta P_{W/A}}{\sigma_{W/A}} \tag{A.2}$$

$$\frac{dZ}{dr} = -\tan\psi \tag{A.3}$$

Here Z is the local distance from the film surface to the horizontal midplane of the foam film, ψ is the running slope angle of the meniscus, r is the radial coordinate, $\Delta P_{W/A} = (P_A - P_W)$ is the capillary pressure drop between the aqueous and the gaseous phases, and $\sigma_{W/A}$ is the surface tension of the aqueous phase (Fig. 1 *B*). The two terms in the left side of Eq. A.2 correspond to the two principal curvatures of the air-water interface ($1/R_1$ and $1/R_2$, respectively) (see Eq. 1).

The set of Eqs. A.2 and A.3 for the two unknown functions, $Z(r)$ and $\psi(r)$, contains one unknown parameter, $\Delta P_{W/A}$. We determine $Z(r)$ and $\psi(r)$ by numerical integration of Eqs. A.2 and A.3, starting from the last outer bright fringe of radius r_1, which corresponds to a film thickness $2Z_1 = (\lambda_0/4n_W) = 102$ nm (see Eq. A.1). The boundary conditions at this fringe can be written in the form

$$Z(r_1) = Z_1; \qquad \psi(r_1) = \psi_1 \tag{A.4}$$

Note that in the boundary conditions A.4, Z_1 is known exactly (Eq. A.1), whereas r_1 and ψ_1 are unknown values that must be determined (along with $\Delta P_{W/A}$) from comparison of the calculated meniscus profile with the measured positions of the interference fringes. A fourth-order Runge-Kutta method (Press et al., 1992) is used to solve Eqs. A.2 and A.3. The merit function

$$\chi^2(r_1, \psi_1, \Delta P_{W/A}) = \sum_{k>1} [Z^{TH}(r_k, r_1, \psi_1, \Delta P_{W/A}) - Z_k^{EXP}]^2 \tag{A.5}$$

is minimized for determination of r_1, ψ_1, and $\Delta P_{W/A}$. Here Z^{TH} is the theoretically calculated function, and Z_k^{EXP} and r_k are determined experimentally from the interference fringes. Summation is carried out over all fringes (outside the contact region) whose radius can be precisely measured. The three adjustable parameters are simultaneously varied by the Marquardt-Levenberg nonlinear least-squares method (Press et al., 1992).

Having found the three parameters ($\Delta P_{W/A}$, r_1, and ψ_1), one can restore the shape of the air-water interface, $Z(r)$, outside the contact region by integration of Eqs. A.2 and A.3, along with the boundary conditions in Eq. A.4. Note that the solution $Z(r)$ thus obtained has an asymptotic character; it describes the shape of the Plateau border around the trapped cell.

Shape of the contact zone (cell-Ab film)

The solution of the Laplace equation of capillarity for the two caps of the cell in the contact zone (AA' and BB' in Fig. 3) represents a portion of a sphere. Its radius of curvature, R_F, can be determined from the inner set of interference fringes by using Eq. A.1 and the equation describing the spherical caps,

$$(Z - p)^2 + r^2 = R_F^2 \tag{A.6}$$

where $Z(r)$ denotes half of the distance between the two opposite spherical caps (Fig. 1); p is the displacement of the center of the sphere with respect to the midplane of the foam film, $z = 0$. R_F and p are determined as adjustable parameters by fitting the data from the inner set of interference fringes (Fig. 1 *A*).

The point of intersection of the spherical caps with the air-water meniscus surrounding the cell gives the coordinates of the contact line, r_C and Z_C, and the slope angles at the contact line, ψ_C and θ_C (Fig. 3). The values of the latter four parameters are obtained numerically.

Shape of the cell-water interface

The shape of the cell membrane, $\zeta(r)$, that is not in contact with the air-water interface (see Fig. 3), is also governed by the Laplace equation of capillarity. For the following consideration, it is more convenient to write Eqs. A.2 and A.3 in their equivalent forms:

$$\frac{d}{dr}\left(\frac{\zeta'}{\sqrt{1+\zeta'^2}}\right)+\frac{\zeta'}{r\sqrt{1+\zeta'^2}}=\frac{\Delta P_{C/W}}{\sigma_C} \qquad (A.7)$$

$$\zeta' \equiv \frac{d\zeta}{dr} \qquad (A.8)$$

where $\zeta(r)$ is the generatrix of the cell membrane, $\Delta P_{C/W} = (P_C - P_W)$ is the capillary pressure drop across the cell membrane, and σ_C is the membrane tension. Because of the symmetry of the system with respect to the plane $z = 0$, we can consider only the upper half of the cell, $\zeta > 0$. Equations A.7 and A.8 can be analytically integrated by using the boundary condition

$$\zeta' = -\infty \qquad \text{at } r = R. \qquad (A.9)$$

The result reads:

$$\frac{d\zeta}{dr}=\frac{b(1-r^2/R^2)-1}{\sqrt{1-r^2/R^2}\sqrt{2b-1-b^2(1-r^2/R^2)}} \qquad (A.10)$$

where b is defined by Eq. 4. An additional integration of Eq. A.10 along with the boundary condition $\zeta(r = R) = 0$ leads to an explicit expression for the shape of the cell membrane, that is, Eq. 2.

The mechanical properties of the membrane are characterized by the tension of the leukocyte cell, σ_C, in Eq. A.7. For red blood cells other characteristics, like the bending elasticity modulus, k_C, and the shearing elasticity modulus, η_C, were found to make some contribution to the total energy of cell deformation (Evans, 1985a,b, 1988). A generalization of the Laplace equation of capillarity, including two additional terms related to the bending and shearing elasticity, k_C and η_C, was recently obtained by a rigorous thermodynamic approach (see equation 4.20 in Kralchevsky et al., 1994). For an axisymmetrical surface, this equation reads:

$$\sigma_C\left(\frac{d\sin\varphi}{dr}+\frac{\sin\varphi}{r}\right)=\Delta P_{C/W} + \frac{k_C}{r}\cos\varphi\frac{d}{dr}\left\{r\cos\varphi\frac{d}{dr}\left[\frac{1}{r}\frac{d}{dr}(r\sin\varphi)\right]\right\} - \eta_C\left(\frac{d\sin\varphi}{dr}-\frac{\sin\varphi}{r}\right) \qquad (A.7')$$

Taking typical values for the elastic constants, $k_C \approx 10^{-19}$ J and $\eta_C \approx 10^{-2}$ mN/m (Evans and Skalak, 1980; Evans, 1988), one can estimate that the last two terms are at least two orders of magnitude smaller compared to the other terms (see the values of σ_C and $\Delta P_{C/W}$ in Table 1). This estimate proves that the effects of bending and shearing elasticity can be neglected in the Laplace equation of capillarity for our system. They could affect the membrane mechanics only in a narrow vicinity of the contact line (where the membrane is strongly curved), thus contributing to the appearance of line tension acting along the contact line. As discussed after Eqs. A.16–A.17 below, we have found that the effect of the line tension is negligible in the framework of experimental accuracy.

The viscous effects can also be neglected in our case, because the typical time scale in our experiments (~60 s) is much longer than the typical relaxation time of the cell deformation (~0.001–1 s; see Evans and Skalak, 1980; Chien et al., 1987). One can estimate that the viscous forces can be neglected in comparison with the capillary force, which deforms the cells in our experiments.

Formulation of the set of equations used for determination of the equatorial radius of the cell, *R*

As mentioned at the end of the third section, the accuracy of the optical measurement of R is insufficient for precise calculation of the other quantities. To overcome this problem, we formulated a set of several equations that must be solved numerically to calculate R and to describe completely the geometry of the system. Moreover, the values of the cell membrane tension, σ_C, the tension of the asymmetrical cell-water-air film, γ, and the capillary pressure, $\Delta P_{C/W}$, are also to be calculated.

The requirement for intersection of the water-air interface with the cell surface at the contact line reads:

$$(Z_C)_{W/A} = \zeta_C \qquad (A.11)$$

where $(Z_C)_{W/A}$ is the height of the water-air interface at the contact line, obtained from the analysis of the outer set of interference fringes, and $\zeta_C \equiv \zeta(r_C)$ is the height of the cell surface at the contact line. From Eq. 2 we obtain

$$(Z_C)_{W/A} = \zeta_C \equiv R[E(\Phi_C, m) - \sqrt{1-m}F(\Phi_C, m)] \qquad (A.12)$$

Another relationship can be found from the Laplace equation of capillarity (Eq. A.7), which describes the shape of the cell membrane outside the contact zone. Equation A.7 can be written in the equivalent form,

$$\sigma_C\frac{1}{r}\frac{d}{dr}(r\sin\varphi)=\Delta P_{C/W} \qquad (A.7'')$$

The integration of Eq. A.7″ over r in the range from R to r_C yields the expression

$$\sigma_C(r_C\sin\varphi_C - R)=\frac{1}{2}\Delta P_{C/W}(r_C{}^2 - R^2) \qquad (A.13)$$

where φ_C is the slope angle of the cell membrane at the contact line (see Fig. 3). The capillary pressure drop across the membrane, $\Delta P_{C/W}$, can be expressed through the capillary pressures at the water-air interface, $\Delta P_{W/A}$, and across the asymmetrical cell-water-air film, $\Delta P_F = 2\gamma/R_F$:

$$\Delta P_{C/W} = \Delta P_F + \Delta P_{W/A} = \frac{2\gamma}{R_F} + \Delta P_{W/A} \qquad (A.14)$$

where γ is the film tension of the cell-Ab film (Fig. 3). Eliminating $\Delta P_{C/W}$ from Eqs. A.13 and A.14, one obtains the following expression:

$$\sigma_C\left(\sin\varphi_C - \frac{R}{r_C}\right)=\frac{r_C^2 - R^2}{2r_C}\left(\frac{2\gamma}{R_F}+\Delta P_{W/A}\right) \qquad (A.15)$$

which is used below in the derivation of the final set of equations.

Two other relations stem from the interfacial tension vectorial balance at the three-phase contact line (Ivanov and Kralchevsky, 1988):

$$\sigma_{W/A}\cos\psi_C + \sigma_C\cos\varphi_C = \gamma\cos\theta_C \qquad (A.16)$$

$$\sigma_{W/A}\sin\psi_C + \sigma_C\sin\varphi_C = \gamma\sin\theta_C \qquad (A.17)$$

where ψ_C and θ_C are the slope angles of the water-air interface and of the cell caps, respectively, at the contact line (see Fig. 3). In principle, this balance could include a term accounting for the line tension. This effect can

be taken into account in our consideration, but it was found with other systems to be relatively small (Ivanov et al., 1992). Furthermore, the presence of a detectable line tension should lead to a variation in the contact angle, α, with the radius of the contact line, r_C. Because we did not find such a dependence (see Table 1), it seems self-consistent to neglect the line tension effect.

The set of four equations A.12, A.15–A.17 contains four unknown quantities: γ, σ_C, φ_C, and R. It was further modified in the following way. From Eqs. A.15 and A.17, and the geometrical relationship

$$\sin \theta_C = \frac{r_C}{R_F} \tag{A.18}$$

one can derive an expression for the film tension, γ,

$$\gamma = a(\sigma_C + d) \tag{A.19}$$

where, by definition,

$$\alpha \equiv \frac{R_F}{R}; \qquad d \equiv \frac{r_C}{R}\left(\sigma_{W/A}\sin \psi_C - \Delta P_{W/A}\frac{R^2 - r_C^2}{2r_C}\right) \tag{A.20}$$

On the other hand, one can express σ_C from Eqs. A.16 and A.17:

$$\sigma_C^2 = \gamma^2 + \sigma_{W/A}^2 - 2\gamma\sigma_{W/A}\cos(\theta_C - \psi_C) \tag{A.21}$$

The substitution of γ from Eq. A.19 into Eq. A.21 leads to a quadratic equation for the membrane tension, σ_C, whose solution is

$$\sigma_C = \frac{1}{a^2 - 1}[a\sigma_{W/A}\cos(\theta_C - \psi_C) - a^2 d \pm D^{1/2}] \tag{A.22}$$

where the discriminant D is given by the expression

$$D = (\sigma_{W/A} - ad)^2 + a\sigma_{W/A}[1 - \cos(\theta_C - \psi_C)] \cdot [2d - a\sigma_{W/A} - a\sigma_{W/A}\cos(\theta_C - \psi_C)] \tag{A.23}$$

It can be proved that the physically meaningful solution of Eq. A.22 is that with a + sign in front of $\sqrt{D}$ (the other solution gives $\sigma_C < (\gamma - \sigma_{W/A})$, which is impossible, because this violates the necessary condition for equilibrium, the existence of the Neumann triangle). Furthermore, the condition $D \geq 0$ guarantees that the value of σ_C is real.

Thus we obtain the final set of four equations, A.12, A.17, A.19, and A.22, for the four unknown quantities, σ_C, γ, φ_C, and R, at a given capillary pressure. The block scheme of the numerical procedure used for solution of this set of equations, and for the complete interpretation of the interference pattern, is shown in Fig. 9. In particular, for a given value of R we calculate σ_C from Eq. A.22. Then $\gamma(R)$ is calculated from Eq. A.19, $\varphi_C(R)$ is calculated from Eq. A.17, and finally, R is obtained by numerically solving Eq. A.12. Note that the quantities γ, σ_C, φ_C, and R are not adjustable parameters in the numerical procedure used—their values are determined as a solution of a complete set of equations. (Adjustable parameters are r_1, ψ_1, and $\Delta P_{W/A}$, which are determined from the fit of the experimental data; see Eq. A.5).

Accuracy of the numerical procedure used for data interpretation

The random error stemming from the limited accuracy in the optical measurements of the radii of the interference fringes can be estimated by analysis of several consecutive images taken within a very short time interval when the values of the parameters should be constant. Comparison of the calculated values from such images shows that the reproducibility is very good for all calculated parameters, within a few percent. However, the comparison of images taken at larger time intervals (~30 s) shows a much larger scattering of the calculated values (see Table 1). This means that the scattering in the results is due mainly to real changes in the living biological cell and/or its interaction with the adsorption layer.

Systematic errors could arise from several sources: from imprecise values of the surface tension $\sigma_{W/A}$, light wavelength, λ, refractive index of the film and the cell, from the slope of the two film surfaces (Eq. A.1 used for analysis of the interference pattern is derived for a plane-parallel film), and some others. All of these systematic errors were estimated to be within the limits of experimental reproducibility.

In conclusion, the accuracy of the optical determination is, in principle, high enough. However, as seen from the values quoted in Tables 1 and 2, there is a substantial scattering of the results, which is due to real changes in the interaction of the biological cell with the adsorption layer. Therefore, the data reported in Table 1 and the confidence intervals in Table 2 are representative of the reproducibility and accuracy of the determined quantities.

Dr. G. Altankov and his collaborators kindly performed the culturing of the cell lines, and their help is gratefully acknowledged. The authors are indebted to Miss R. Dimova and Mrs. S. Cholakova for their help in the numerical analysis of part of the data.

REFERENCES

Abbas, A. K., A. H. Lichtman, and J. S. Pober. 1994. Cellular and Molecular Immunology, 2nd Ed. Saunders, London.

Abramowitz, M., and I. A. Stegun. 1964. Handbook of Mathematical Functions, Applied Mathematics Series, Vol. 55. National Bureau of Standards, Washington, DC (reprinted by Dover Publications, New York, 1968).

Acuto, O., R. E. Hussey, K. A. Fitzgerald, J. P. Protentis, S. C. Meuer, S. F. Schlossman, and E. L. Reinherz. 1983. The human T cell receptor: appearance in ontogeny and biochemical relationship of α and β subunits on IL-2 dependent clones and T cell tumors. *Cell.* 34:717–726.

Adamson, A. 1976. Physical Chemistry of Surfaces, 3rd Ed. Wiley-Interscience, New York.

Alberts, B., D. Bray, J. Lewis, M. Raff, K. Roberts, and J. D. Watson. 1994. Molecular Biology of the Cell, 3rd Ed. Garland Publishing, New York.

Alcover, A., C. Alberini, O. Acuto, L. K. Clayton, C. Transy, G. C. Spagnoli, P. Moingeon, P. Lopez, and E. L. Reinherz. 1988. Interdependence of CD3-Ti and CD2 activation pathways in human T lymphocytes. *EMBO J.* 7:1973–1977.

Bell, G. I. 1978. Models for the specific adhesion of cells to cells. *Science.* 200:618–627.

Bell, G. I. 1988. Models of cell adhesion involving specific binding. *In* Physical Basis of Cell-Cell Adhesion. P. Bondgrand, editor. CRC Press, Boca Raton, FL. 227–258.

Bell, G. I., M. Dembo, and P. Bongrand. 1984. Cell adhesion: competition between nonspecific repulsion and specific bonding. *Biophys. J.* 45: 1051–1064.

Bongrand, P., editor. 1988. Physical Basis of Cell-Cell Adhesion. CRC Press, Boca Raton, FL.

Bongrand, P., C. Capo, J.-L. Mege, and A.-M. Benoliel. 1988. Use of hydrodynamic flows to study cell adhesion. *In* Physical Basis of Cell-Cell Adhesion. P. Bondgrand, editor. CRC Press, Boca Raton, FL. 125–156.

Born, M., and E. Wolf. 1993. Principles of Optics, 6th Ed. Pergamon Press, Oxford.

Chien, S., K.-L. P. Sung, G. W. Schmid-Schonbein, R. Skalak, E. A. Scmalzer, and S. Usami. 1987. Rheology of leukocytes. *Ann. N.Y. Acad. Sci.* 516:333–347.

Cozens-Roberts, C., J. A. Quinn, and D. A. Lauffenberger. 1990. Receptor-mediated adhesion phenomena: model studies with the radial-flow detachment assay. *Biophys. J.* 58:107–125.

Darnell, J., H. Lodish, and D. Baltimore. 1990. Molecular Cell Biology, 2nd Ed. Scientific American Books, New York.

de Feijter, J. A. 1988. Thermodynamics of thin liquid films. *In* Thin Liquid Films. I. B. Ivanov, editor. Marcel Dekker, New York. 1–48.

Denkov, N. D., H. Yoshimura, and K. Nagayama. 1996. Method for controlled formation of vitrified films for cryo-electron microscopy. *Ultramicroscopy.* 65:147–158.

Derjaguin, B. V. 1989. Theory of Stability of Colloids and Thin Liquid Films. Plenum Press, Consultants Bureau, New York.

Evans, E. 1985a. Detailed mechanics of membrane-membrane adhesion and separation. I. Continuum of molecular cross-bridges. *Biophys. J.* 48:175–184.

Evans, E. 1985b. Detailed mechanics of membrane-membrane adhesion and separation. II. Discrete, kinetically trapped molecular cross-bridges. *Biophys. J.* 48:185–191.

Evans, E. 1988. Micropipette studies of cell and vesicle adhesion. *In* Physical Basis of Cell-Cell Adhesion. P. Bondgrand, editor. CRC Press, Boca Raton, FL. 173–190.

Evans, E., and R. Skalak. 1980. Mechanics and Thermodynamics of Biomembranes. CRC Press, Boca Raton, FL.

Fisher, L. 1993. Forces between biological surfaces. *J. Chem. Soc. Faraday Trans.* 89:2567–2582.

Foa, C., J.-L. Mege, C. Capo, A.-M. Benoliel, R. Galindo, and P. Bongrand. 1988. Electron microscopic study of the surface topography of isolated and adherent cells. *In* Physical Basis of Cell-Cell Adhesion. P. Bondgrand, editor. CRC Press, Boca Raton, FL. 191–206.

Hadjiiski, A., R. Dimova, N. D. Denkov, I. B. Ivanov, and R. Borwankar. 1996. Film trapping technique: a precise method for contact angle determination of solid and fluid particles. *Langmuir.* 12:6665–6675.

Hammer, D. A., and D. A. Lauffenburger. 1987. A dynamic model for receptor-mediated cell adhesion to surfaces. *Biophys. J.* 52:475–487.

Hussey, R. E., L. K. Clayton, A. Diener, D. J. McConkey, F. D. Howard, H.-R. Rodewald, L. D'Adamio, F. Dallenbach, H. Stein, E. V. Schmidt, S. Koyasu, and E. L. Reinherz. 1993. Overexpression of CD3η during thymic development does not alter the negative selection process. *J. Immunol.* 150:1183–1194.

Israelachvili, J. N. 1992. Intermolecular and Surface Forces, 2nd Ed. Academic Press, New York.

Ivanov, I. B., and P. A. Kralchevsky. 1988. Mechanics and thermodynamics of curved thin liquid films. *In* Thin Liquid Films. I. B. Ivanov, editor. Marcel Dekker, New York. 49–130.

Ivanov, I. B., P. A. Kralchevsky, A. S. Dimitrov, and A. D. Nikolov. 1992. Dynamics of contact lines in foam films. *Adv. Colloid Interface Sci.* 39:77–101.

Ivanov, I. B., and B. V. Toshev. 1975. Thermodynamics of thin liquid films. I. Basic relations and conditions for equilibrium. II. Film thickness and its relations to the surface tension and the contact angle. *Colloid Polym. Sci.* 253:558–565, 593–599.

Kralchevsky, P. A., K. D. Danov, and N. D. Denkov. 1997. Chemical physics of colloid systems and interfaces. *In* Handbook of Surface and Colloid Chemistry. K. S. Birdi, editor. CRC Press, Boca Raton, FL. 333–494.

Kralchevsky, P. A., K. D. Danov, and I. B. Ivanov. 1995. Thin liquid film physics. *In* Foams: Theory, Measurements, and Applications. R. K. Prud'homme and S. A. Khan, editors. Marcel Dekker, New York. 1–98.

Kralchevsky, P. A., J. C. Eriksson, and S. Ljunggren. 1994. Theory of curved interfaces and membranes: mechanical and thermodynamical approaches. *Adv. Colloid Interface Sci.* 48:19–59.

Leckband, D. E., F.-J. Schmidt, J. N. Israelachvili, and W. Knoll. 1994. Direct force measurements of specific and nonspecific protein interactions. *Biochemistry.* 33:4611–4624.

Mescher, M. F. 1992. Surface contact requirements for activation of cytotoxic T lymphocytes. *J. Immunol.* 149:2402–2405.

Meuer, S. C., J. C. Hodgdon, R. E. Hussey, J. P. Protentis, S. F. Schlossman, and E. L. Reinherz. 1983. Antigen-like effects of monoclonal antibodies directed at receptors on human T cell clones. *J. Exp. Med.* 158:988–993.

Princen, H. M. 1969. The equilibrium shape of interfaces, drops, and bubbles. Rigid and deformable particles at interfaces. *In* Surface and Colloid Science, Vol. 2. E. Matijevic, editor. Wiley-Interscience, New York. 1–84.

Press, W. H., S. A. Teukolsky, W. T. Vetterling, and B. P. Flannery. 1992. Numerical Recipes in C. The Art of Scientific Computing, 2nd Ed. Cambridge University Press, New York.

Scheludko, A., and D. Exerowa. 1959. Über den elektrostatischen durck in schaumfilmen aus wässerigen elektrolytlösungen. *Kolloid-Z.* 165: 148–151.

Weiss, A. 1993. T lymphocyte activation. *In* Fundamental Immunology, 3rd Ed. W. E. Paul, editor. Raven Press, New York. 467–503.